Substituent Effect on *g*-Tensor: Multifrequency ESR Study and DFT Calculation of Polycrystalline Phenoxyl Radicals in Diamagnetic Crystals

Toshiki Yamaji,*,† Islam SM Saiful,‡ Masaaki Baba,† Seigo Yamauchi,‡ and Jun Yamauchi†

Department of Chemistry, Graduate School of Science, Kyoto University, Oiwake-cho, Kitashirakawa, Kyoto 606-8502, Japan, and Institute of Multidisciplinary, Research for Advanced Materials, Tohoku University, Katahira 2-1-1, Aoba-ku, Sendai 980-8577, Japan

Received: February 14, 2007; In Final Form: March 11, 2007

The substituent effect on the *g*-tensor of polycrystalline 2,6-di-*tert*-butyl phenoxyl radical derivatives diluted in diamagnetic crystals was investigated using multifrequency ESR spectroscopy and DFT calculations. It was revealed that the *g*-tensors of the series of phenoxyl radical derivatives essentially have an orthorhombic symmetry. For some radicals, the hyperfine-splitting tensors from the para groups were resolved. The interpretations and the assignments of the spin-Hamiltonian parameters were confirmed with computer simulations in all bands. The DFT-calculated *g*-tensors were consistent with the experimental *g*-tensors. Furthermore, the shifts Δg from the free electron g_e were analyzed in details as the sum of three contributions. The spin−orbit interactions were found to be the dominant factor with regard to the Δg. With a focus on the s−o term, thus, the relationship of the *g*-values and the electronic excited states was explained by visualizing the molecular orbitals of the phenoxyl radical derivatives. This study thus showed the very significant potential of the combination of a multi-frequency ESR approach and a DFT calculation to advanced ESR analysis, particularly, *g*-tensor analysis, even for a powder-sample radical.

1. Introduction

g-values might be the most fundamental parameter on magnetic resonance spectroscopy. Except for zero-magnetic-field experimental studies, *g*-factors (Zeeman terms) always appear in spin-Hamiltonians. For Electron Spin Resonance (ESR), however, the interpretation of the ESR *g*-value is particularly complex. Furthermore, the amplitude of its change is generally too small, and the shift from the *g*-value of the free electron ($g_e = 2.002319...$) is also too small due to the quench of the orbital angular momentum, especially, for organic radicals or *S*-state transition metals. Thus, it is very difficult to make the best use of the *g*-value for a detailed and quantitative quantum-physical-chemical analysis of organic radicals. The *g*-value naturally can be used to obtain detailed information about the radicals themselves and their local structure.

The quantum-chemical theory of *g*-factors for organic radicals was first developed by Stone,[1,2] using the molecular orbital method based on a Hückel description of the electronic structures of the radicals. A large number of studies of the effects of solvents on isotropic *g*-values were carried out later, mainly for nitroxyl radicals,[3−6] which are relatively stable and useful for spin-trapping, spin-labeling and spin-probing methodologies.

Incidentally, with the advent of high-field ESR techniques, it has become possible to assess the *g*-tensors of organic radicals. One of the driving forces in the development of high-field ESR has been the ability to accurately measure the small *g*-anisotropies that characterize most organic radicals. Accurate *g*-values of radicals in biological[7,8] and photo-or electro-catalytic[9] systems have been measured.

From the Gaussian 03 version,[10] which is an ab initio calculation program package, the subroutine of the calculation of *g*-values has been contained. Therefore, the experimental researchers also have been able to conduct more detailed and quantitative analysis by comparing the calculated *g*-values with the experimentally obtained data. Moreover, the Gaussian 03's output also contains a more detailed *g*-shift from g_e divided into the three components (the relativistic mass correction, the diamagnetic correction, and the cross term between the orbital Zeeman (OZ) and the spin−orbit coupling (SOC) operators), which, at present, are very difficult or impossible to observe in experiments (for example, the *g*-shift from g_e is only accessible in experiments.).

In *The Journal of Physical Chemistry A*,[11] we recently reported a multi-frequency ESR study of the polycrystalline phenoxyl radical of α-(3,5-di-*tert*-butyl-4-hydroxyphenyl)-N-*tert*-butylnitrone in the diamagnetic matrix, which is very useful as a spin-trapping technique. As reported, we successfully interpreted the powder-pattern ESR spectra and assigned the ESR parameters (*g*-tensor and hyperfine tensor) using high-frequency ESR (Q- and W-band ESR) techniques beyond the conventional X-band ESR. The *g*-anisotropy was qualitatively but reasonably explained with the resonance structure of the radical using the *g*-tensors data of the 2,4,6-tri-*tert*-butyl phenoxyl radical (as is well-known, a TTBP radical) and the di-*tert*-butyl nitroxyl radical (a DTBN radical), which were chosen as model phenoxyl and nitroxyl radicals, respectively. The study, thus, showed the significant potential of a multi-frequency ESR approach to powder-sample radicals, in particular, samples that are difficult to acquire as single crystals because of their high resolution with a *g*-value, confirming the electronic structure of the phenoxyl radical in terms of the ESR parameters.

* Corresponding author. Tel: +81-75-753-4012. Fax: +81-75-753-4000. E-mail: toshiki-y@nirvana.mbox.media.kyoto-u.ac.jp.
† Kyoto University.
‡ Tohoku University.

10.1021/jp071263j CCC: $37.00
Published on Web 05/10/2007

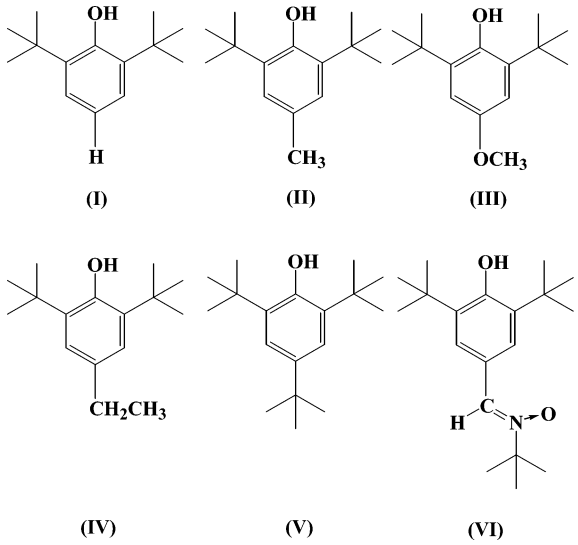

Figure 1. Structural formulas of the phenol parent compounds corresponding to the phenoxyl radicals discussed in this work. The corresponding phenoxyl radicals are referred to in the text as (I′) 4htbp′, (II′) 4mtbp′, (III′) 4motbp′, (IV′) 4etbp′, (V′) TTBP′, and (VI′) spin trap′.

SCHEME 1: Oxidation Scheme of the Sample

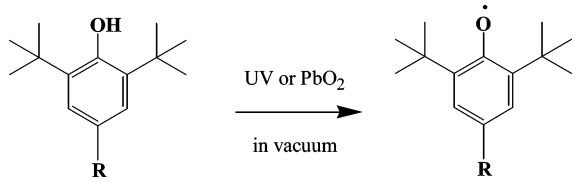

At this point, we have systematically interpreted the powder-pattern ESR spectra of a series of the phenoxyl radical derivatives with *tert*-butyl groups at both para positions, including the above radical, and obtained the *g*-tensors data from X-, Q-, and W-band multifrequency ESR investigations. In the present work, we have combined those experimental data with DFT calculations for a detailed and quantitative study of the substituent effect on the *g*-tensors of the phenoxyl radical derivatives. Here, we report the mechanism of the substituent effect on the *g*-values of the phenoxyl radical derivatives at the tensor level, dividing the *g*-shifts into three contributions. Moreover, from the view of the molecular orbitals of the radicals, by focusing on the mechanism of the spin−orbit interactions, the correlation of the *g*-values and the electronic excited states is discussed.

2. Materials and Methods

As shown in Figure 1, (I) is 2,6-di-*tert*-butyl-phenol, and (II), (III), (IV), (V), and (VI) are 2,6-di-*tert*-butyl-4-methyl-phenol, 2,6-di-*tert*-butyl-4-methoxy-phenol, 2,6-di-*tert*-butyl-4-ethyl-phenol, 2,4,6-tri-*tert*-butyl-phenol, and α-(3,5-di-*tert*-butyl-4-hydroxyphenyl)-N-*tert*-butylnitrone, respectively. I−VI are referred to in the text as 4htbp, 4mtbp, 4motbp, 4etbp, TTBP, and spin trap, respectively.

Precursor phenols purchased commercially (I−V) or synthesized following the procedure described in the literature[12] (VI[11]) were recrystallized from a toluene solution at room-temperature several times and UV-irradiated in vacuo for 4 or 5 h for the radical generation with a high-pressure mercury lamp manufactured by Ushio Electric Inc (shown in Scheme 1)[13−15]. It was found that these generated radicals are dispersed homogeneously in the diamagnetic matrixes of the corresponding phenols,[14,15] just like the system of γ-irradiation.[16] On the other hand, it was found that the oxidation reactions with chemical reagents such as lead dioxide or potassium ferricyanide yield almost quantitatively the corresponding radicals through abstraction of a hydrogen atom from a phenoric hydroxyl group.

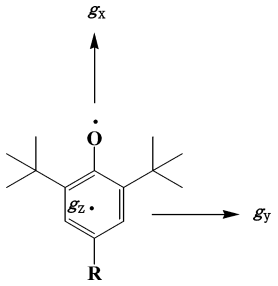

Figure 2. Orientation of the *g*-tensor in the phenoxyl radicals.

It was confirmed that both methods could produce the corresponding phenoxyl radicals diluted in the diamagnetic crystals, i.e., the primary phenol,[11,15] giving the same ESR spectra. (I′) can be obtained only by UV irradiation, since, in solution, the generated (I′) can instantly dimerize (as shown in Scheme 2), becoming diamagnetic and ESR-silent. Each sample was sealed in a 5 mm φ X-band ESR sample tube in a vacuum. The results of the samples obtained by UV irradiation are shown in this paper.

3. Experimental and Simulations

X- and Q-band ESR experiments were carried out using a JEOL FE1XG or RE3X spectrometer and a JEOL FE-3X ESR spectrometer, respectively. W-band ESR measurements were performed using a Bruker E600 W-band EPR spectrometer at the laboratory of Prof. Seigo Yamauchi in Tohoku University. All experiments were carried out at room temperature. X-band ESR experiments were conducted with the samples in the vacuated X-band tubes, whereas Q- and W-band measurements were carried out with the samples in the Q- and W-band tubes not vacuated after taking the samples out of the X-band tubes. In this work, the effect of air was not considered to be a problem. Sealing the X-band tube also contributed to maintain the vacuum before high-frequency ESR measurements. After the experimental results had been interpreted and assigned, computer simulations of the ESR spectra were conducted with the assigned spin-Hamiltonian parameters using Bruker Simfonia V.1.25.

4. Results of ESR Spectra and Simulations

The orientation of the *g*-tensor in the phenoxyl radicals can be defined as illustrated in Figure 2.[7,8,17,18]

The experimental (solid lines) and simulated (dotted line) W-band ESR spectra of the radicals are shown in Figures 3. The experimental (solid lines) and simulated (dotted lines) all-band ESR spectra of the radicals are shown in Figures S1−S6 (Supporting Information). In the experimental W-band spectra, the assignments of the *g*- and hyperfine tensors are also presented.

Tables S1a (Supporting Information) exhibit the obtained experimental *g*-tensors. As in Figures S1−S6, it is very difficult or impossible to analyze the powder-pattern spectra of the samples through the results of the X- or Q-band ESR measurements. Because of the higher resolution with a *g*-value about 10 or 2.5 times than obtained through X- or Q-band ESR spectroscopy, respectively, the W-band ESR spectra enabled

SCHEME 2: Dimerization Scheme of the 4htbp′

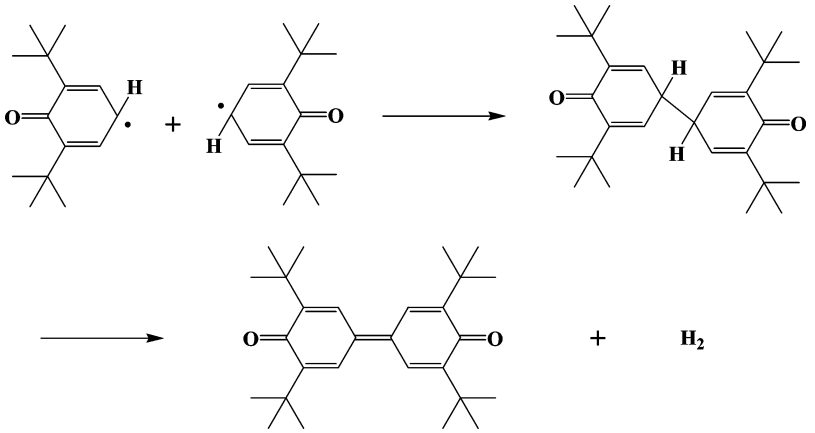

us to interpret powder-pattern spectra that were unresolved in the X- or Q-band measurements.

The W-band spectra show that the phenoxyl radical derivatives in this study exhibit an essentially rhombic symmetry of the *g*-tensors ($g_x > g_y > g_z$). In addition, for (I′), (II′), (IV′), and (VI′), the hyperfine structures from the nuclear in the para groups are resolved and correctly assigned. Those hyperfine-tensor data are summarized in Table S2a (Supporting Information). Moreover in Table S2b (Supporting Information), the isotropic hyperfine-splitting data obtained in the solution experiments are also summarized.

For the calculation of a hyperfine-splitting constant, DFT methods are also considered to be powerful tools.[26] In the case of (VI′), since the $A_\perp$ ($=A_{x,y}$) is unresolved, it was calculated using the A_z and A_{iso} obtained from the solution spectrum.[11] The proton-hyperfine at the methyl group of II′ is resolved, whereas that at the methoxy group of III′ is not. This is consistent with the result of the solution experiments that is not presented here. In the case of I′, A_x is not resolved, unlike the other components, due to the relatively small splitting within the line width. As illustrated in Scheme 2, since the data of I′ in the solution, i.e., the isotropic parameters, could not be obtained, the A_x was reasonably evaluated using the other components and the isotropic value estimated with the DFT calculation, giving the best Simfonia simulation spectra. On the other hand, as shown in Tables S2a and S2b, the average values of the *A*-tensors assigned in the W-band powder-spectra are consistent with the isotropic values obtained in the solution experiments. Furthermore, we concluded that the hyperfine-splitting values (the tensors and the isotropic values) calculated by the DFT are successfully close to the experimental data. Since the primary focus of the present study is not the hyperfine, the details are not shown.

As seen from the W-band experimental spectra, there are other peaks between the perpendicular region and the high-field *g*-feature. From additional investigations, it was concluded that the peaks are due to the crystal part not being fully ground; in other words, the unground spectrum could be compared with the ground spectrum in the present work. Thus, it may be concluded that peaks resulting from a very small amount of crystal that cannot be completely ground to powder are noticeable in W-band or higher-frequency ESR spectra.[11]

5. Density Functional Calculation Method and Results

All DFT calculations were performed using the Gaussian 03 program[10] to estimate the spin-Hamiltonian parameters. After the structure of the radicals had been optimized, the parameters were evaluated. The B3LYP method and the 6-31G(d) basis set were used for both the structure optimizations and the ESR-parameter calculations. The B3LYP method is known to be applicable for the calculations of organic radicals as well as transition metal ions.[17,19,20] In this work, the UB3LYP/6-31G(d) was compared with some other simple methods or basis-sets. It was revealed that the UB3LYP/6-31G(d) could also be reasonably used for our purpose. The details are not shown here. The *g*-tensors and the shifts Δg from the free-electron value were calculated. Consequently, the validity of this experimental study was confirmed by quantum-chemical calculations.

Figure 4 illustrates the experimental and calculated *g*-tensors as a function of the para groups in the order of the magnitude of spin density on the phenoric oxygen obtained from the structure optimizations of the DFT calculations. Tables S1b list the *g*-tensors obtained from the DFT calculations.

As shown in Figure 4, the data for the DFT calculations was close to that of the experimental *g*-tensors. It is noteworthy that the calculations successfully reproduced the variation of the *g*-tensors as a function of the para groups. A slight degree of error is systematically observed and might be the result of the optimized molecular structures. Another reason might be that the present calculation model is a simple one (isolated)-molecular-type that does not consider the molecular environmental effects, such as the van der Waals force, polarization, and steric strain from the neighboring diamagnetic phenol or paramagnetic radical molecules. Nevertheless, the DFT method (in this work, UB3LYP/6-31G(d)) is a good tool for calculating the *g*-tensor of phenoxyl-type radicals that are possibly more difficult to treat than nitroxyl-type radicals.

Only a *g*-shift itself can be available from an ESR experiment; however, the Gaussian 03 program can produce outputs dividing a total *g*-shift into three contributions. In the following section, the detailed mechanism of the substituent effect of the para groups on the *g*-tensors is discussed at the tensor level.

6. Discussion and Analysis

6.1. The *g*-Shifts at the Tensor Level Divided into Three Contributions. It is well known[1,8,9,17,19−22] that the *g*-tensor can be written as a correction to the free electron value (given in ppm), i.e.

$$g = g_e\delta + \Delta g \qquad (1)$$

and we focus on the *g*-shift (Δg components). Throughout this work, *g*-shifts are given in parts per million. Up to the level of second-order perturbation theory, the *g*-shift consists of the

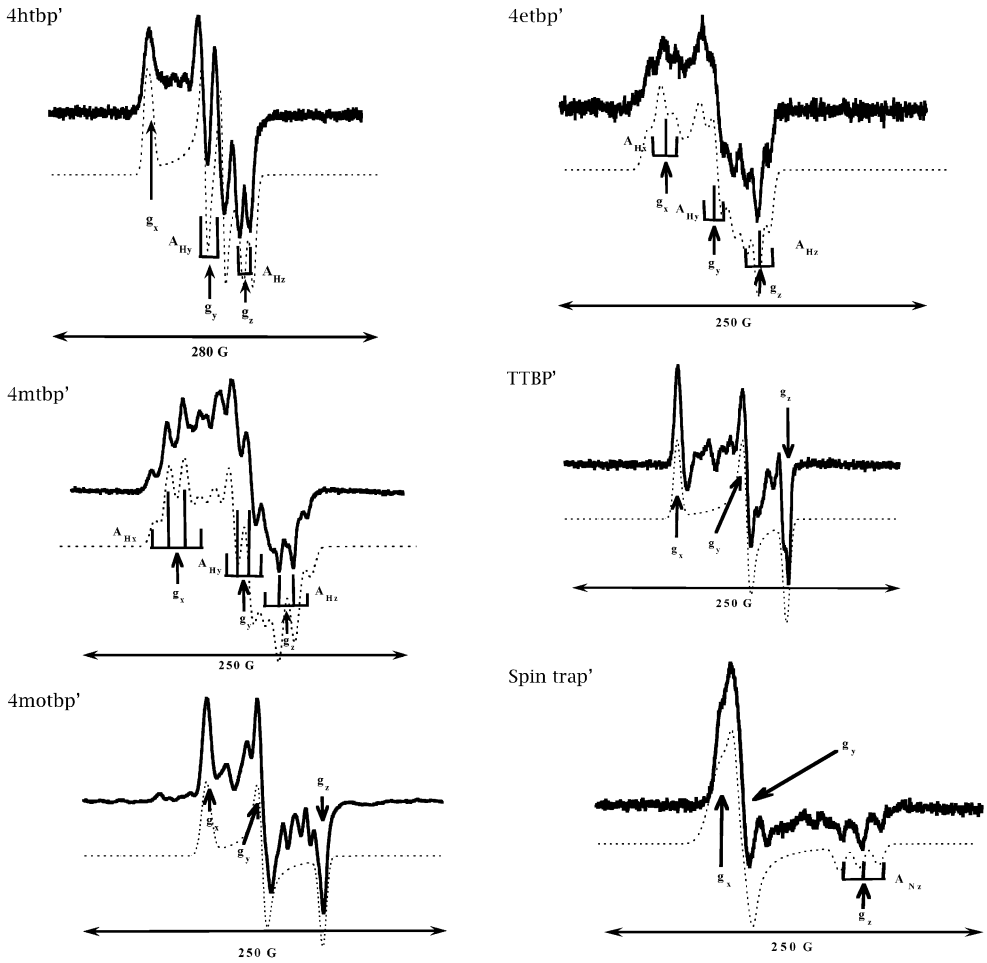

Experimental conditions:	microwave frequency / GHz	center field / G	modulation amplitude / G	microwave power / mW
4htbp'	93.734766	33411.5	10	0.04
4mtbp'	93.853861	33451.5	2	0.1265
4motbp'	93.726025	33401.5	1	0.004
4etbp'	93.753431	33441.5	10	0.1265
TTBP'	93.734766	33411.5	10	0.04
Spin trap'[11]	93.642789	33371.5	5	0.04

The modulation frequency used in the ESR measurements is all 100 kHz.

Figure 3. Experimental (solid lines) and simulated (dotted lines) W-band ESR powder-pattern spectra of the radicals.

relevant Breit-Pauli terms

$$\Delta g = \Delta g_{\mathrm{RMC}}\delta + \Delta g_{\mathrm{DC}} + \Delta g_{\mathrm{OZ/SO}} \qquad (2)$$

where δ is the unit matrix.

The first term is of first order and is due to the relativistic mass correction.[21] The second term is a diamagnetic correction.[1] It is also of first order.[25] Finally, the third is the spin−orbit orbital Zeeman cross term. In the Gaussian 03 program, the calculation method by Neese[19] is employed for the evaluation of the term using the effective nuclear charges and the effective spin−orbit or orbital Zeeman operators estimated by Koseki et al.[25] Here, the theoretical or computational details are not shown (see the references[19,20]). A gauge, including the atomic orbital (GIAO) method, which is included in Gaussian 03, was used for the UB3LYP functional in this work.

The detailed breakdowns of the contributions to the *g*-tensors calculated are summarized in Tables S3 (Supporting Information). In Figures 5, each of the *g*-corrections of the *x*-, *y*-, and z-components and the average are shown together with the experimental values.

It was confirmed that the spin−orbit orbital Zeeman cross term is dominant to the *g*-tensors for the phenoxyl radical

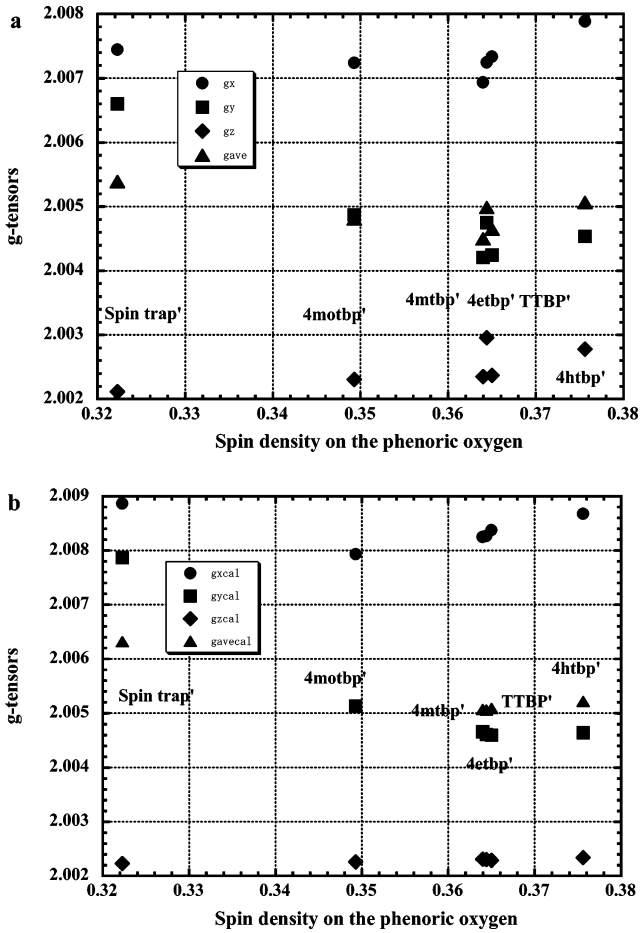

Figure 4. Experimental (a) and calculated (b) *g*-tensors as a function of the para groups in the order of the magnitude of the spin density on the phenoric oxygen.

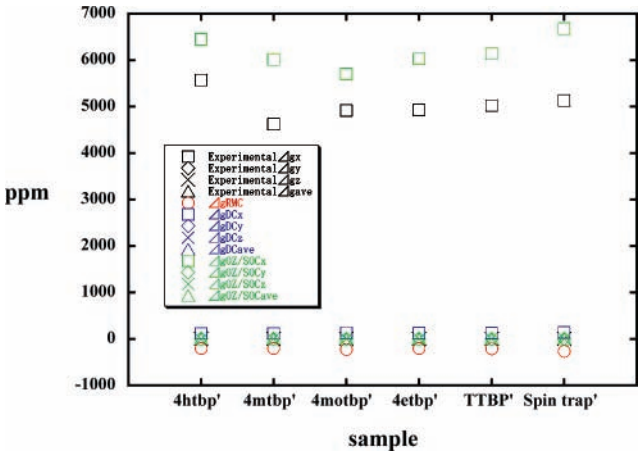

Figure 5. *x*-, *y*-, *z*-components and average values of the experimental Δg and the three corrections from the DFT calculations as a function of the para groups.

derivatives in this study, as is well-known for many other paramagnetic species. The relativistic mass corrections are relatively small and have a negative sign that is characteristic of a π-electron. The diamagnetic current corrections are also small and cancel the contributions from the relativistic mass corrections. The *g*-shifts at the *z*-direction are 1 order smaller than the *x*- and *y*-components. Figure 5 shows that the spin−orbit interactions, to some extent, can contribute to the *g*-shifts at the *z*-direction but are cancelled with the relativistic mass corrections, resulting in $g_z \approx g_e$. In the next section, therefore, by focusing on the perturbation due to the spin−orbit interactions, the investigation of the correlation between the ground state and the excited states that influence the *g*-values is undertaken from the point of view of the molecular orbitals of the phenoxyl radical derivatives.

6.2. Visualized Molecular-Orbital Analysis of the *g*-Shifts. The relation between the *g*-shifts and the excited states is discussed from the point of view of the molecular orbitals of the phenoxyl radical derivatives. The molecular orbitals were visualized on the basis of the output data of the DFT calculations using Gauss View 3.0, the graphical user interface (GUI, graphical soft) of the Gaussian program. Hereafter, we can discuss the present topic using the results of the 4htbp′, since the molecular orbitals of the other phenoxyl radical derivatives are similar to the 4htbp′.

In Figure 6, the five molecular orbitals of 4htbp′ visualized by the Gauss View 3.0 program are shown in the order of the energy level. Those orbitals may be labeled by the bonding σ (σ), the bonding π (π), the nonbonding (n), the antibonding π^* (π^*), and the antibonding σ orbital (σ^*).

A large amount of density of the nonbonding electron pair can be found to be located at the p_y orbital of the oxygen that lies in the plane of the phenyl ring, as seen in Figure 6d. As is discussing in the following, the nonbonding electron at the y-direction dominantly influences the variation of the *x*-components of the *g*-tensors as a function of the para groups, through the n−π^* electron transition. The energy diagram of the 4htbp′ based on the calculation results, therefore, is illustrated in Figure 7. The unpaired electron is in the π^* orbital. That is, the π^* orbital is the SOMO of the phenoxyl radicals in this study.

As seen in Figure 7, the energy of the π orbital is relatively higher due to the conjugation of the two π bonds. The n orbital is coupled with the σ orbitals, resulting in lower energy. In addition, the lowest, second-lowest, and third-lowest electronic transition can be easily understood to be n−π^*, π−π^*, and σ−π^*, respectively. These phenomena are well-known for aromatic carbonyl molecules.

Excited states resulting as an electronic transition between a SOMO and orbitals near a SOMO can dominantly influence *g*-values through spin−orbit couplings. As seen in Figure 7, the excited states resulting as the electronic transitions from the SOMO to the upper unoccupied orbitals (for example, π^*−σ^*), therefore, can be ignored. It may be concluded that the only excited states resulting as the transitions from the inner doubly occupied orbitals to the SOMO (σ(54th) −π^*(57th), π-(55th) −π^*(57th), and n(56th)−π^*(57th)) are to be considered. Since the important excited states are those in which an electron promoted into the SOMO, the *g*-values should be greater than g_e.[25]

In Figure 8, the electronic-transition energies are shown for all samples in the order of the spin density of the oxygen.

It can be understood that, because the σ and n orbitals are in the *x*- and *y*-directions, the σ−π^* and the n−π^* excited states influence Δg_y and Δg_x, respectively. In Figure 4a, the variations of the electronic transition energies are clearly found to be inversely proportional to those of the g_x. Since the n−π^* transition is between the inner orbital and the SOMO, the excited-state can make the g_x larger ($\Delta g_x > 0$). It may, therefore, be concluded that, if the para group R could increase the n−π^* transition energy (ΔE(n−π^*)), the magnitude of the g_x would in turn be reduced and, if the R could decrease the energy, it would in turn be increased. On the other hand, from Figures 4a

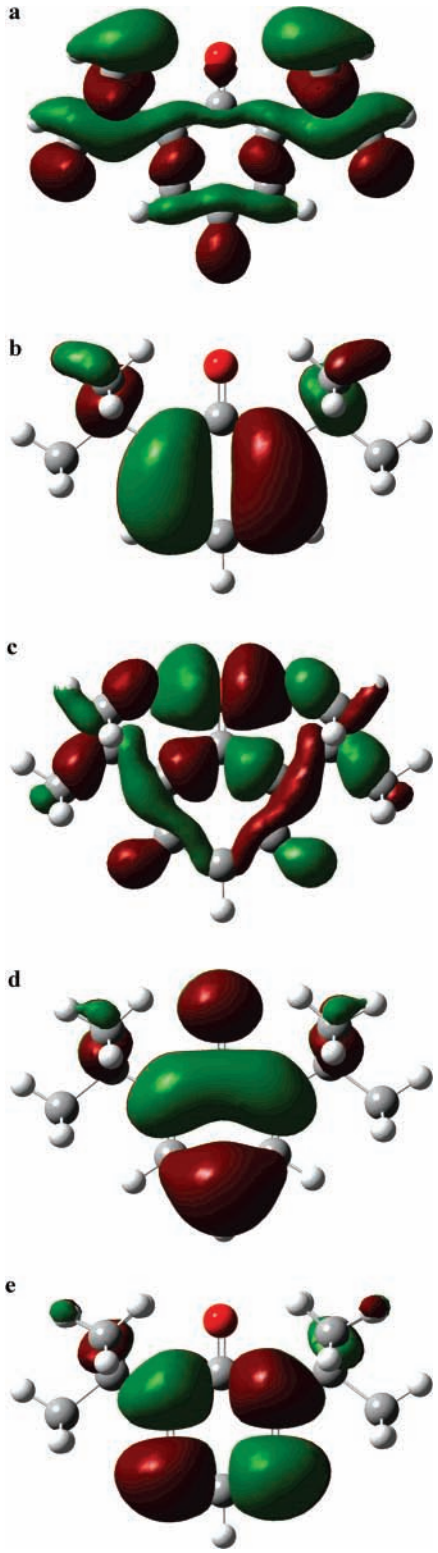

Figure 6. Molecular orbitals of 4htbp′ visualized using the Gauss View 3.0 program. (a) The 54th orbital (σ), (b) the 55th orbital (π), (c) the 56th orbital (n), (d) the 57th orbital (π^*), which is the singly occupied molecular orbital (SOMO), and (e) the 58th orbital (σ^*).

and 8, the relationship of the variation of the g_y and the $\sigma-\pi^*$ excited-state is also successfully explained in the same way. It is concluded that, the g_x (Δg_x) is greater than the g_y (Δg_y), since the ΔE(n-π^*) is lower than the $\Delta E(\sigma-\pi^*)$, and the variation of the g_x is smaller than that of the g_y as a function of the para groups, since the variation of the $\Delta E(n-\pi^*)$ is smaller than that $\Delta E(\sigma-\pi^*)$ as a function of the para groups. It may,

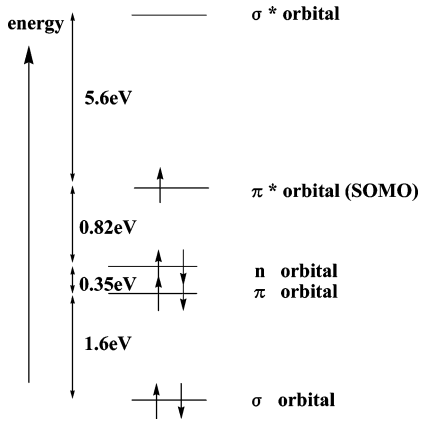

Figure 7. Energy diagram of the 4htbp′ based on the calculation result. The unpaired electron is in the π^* orbital.

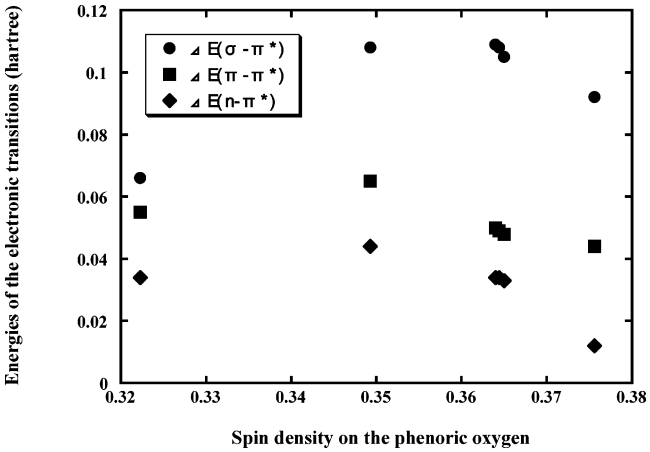

Figure 8. Electronic transition energies of the phenoxyl radical derivatives.

moreover, be concluded that the $\pi-\pi^*$ excited-state may influence the magnitude of the g_z but the π orbital characteristically does not almost cause the spin−orbit interaction and do not influence the g_z-value, resulting in $g_z \approx g_e$. As is seen, the discussion of excitation energy contributions used here is relatively simple, based on orbital energy differences, but is reasonably complete. For a strict analysis, effects such as electron correlations must be also considered, based on state energy differences.

When a spin−orbit interaction is evaluated, s−o coupling constants of each atom also naturally must be considered. However, it was found in this study that the substituent effect on the *g*-tensors of a series of the phenoxyl radical derivatives is successfully explained with the electronic transition energies ΔE. It may be concluded that, though the 4motbp′ and the Spin trap′ contain the heteroatoms (O or N) of which the s−o coupling constants are larger than those of the hydrocarbons, the effect of the heteroatoms is in the degrees of the molecular-orbital coefficient of the atoms and can be ignored in this study. If investigated molecules contain heavier atoms such as halogen atoms, however, the large s−o coupling constants (in other word, heavy-atom effect) must be considered.

The relation "the perpendicular components (g_x and g_y) > the parallel component (g_z)" shows that the unpaired electron is a π electron.[11] Thus, the definition of the orientation of the *g*-tensor in the phenoxyl radicals was also confirmed in this study.

6.3. Additional Comments. *Electronic Structure (Spin-Density Distributions) from the Viewpoint of the* g*-Tensor*. The

relationship between the spin density distributions and *g*-values (isotropic) in semiquinones has been reported.[23] From a study of several semiquinone systems, it was shown that their *g*-values can be expressed in terms of the π-electron spin densities on the oxygens by a linear equation (recognized from Stone's theoretical treatment[1,24]), suggesting the possibility of estimating the spin densities on the oxygens directly from the *g*-values in similar systems. In this present study, from Figure 4, the spin densities on the oxygens for radicals having the hydrocarbon groups at the para position show a linear relation with the *g*-values, similarly to semiquinones.[23] However, the relation of the 4motbp′ and the Spin trap′ containing an oxygen or nitrogen in the para groups does not seem to be applicable. With an additional term, the *g*-values of radicals containing an N, O, or heavier atom could also be given by a linear equation such as that in ref 23. If hetero atoms are not contained in molecules, indeed, *g*-values can be evaluated by the linear relation of spin densities on oxygens such as that in ref 23 (semiquinones); in other word, the Stone's theory is applicable. The simple linear relation cannot, however, be applicable to molecules in which contain hetero atoms. It is obvious that the variation of *g*-values (isotropic) as a function of the para groups may be explained by the magnitude of the spin densities on the oxygens only for hydrocarbon molecules but the real mechanism is not as simple as the reference.

In section 6.2, it was revealed that the substituent effect on the *g*-values of the phenoxyl radical derivatives is successfully explained in the tensor level from the point of view of the separation of the electronic transition energies considering the relationship between the directions of the s−o interactions and those of the wavefunctions of the excited states. On the other hand, in Figure 4, for the *z*-components, since the spin−orbit interaction itself is nearly zero, the linear relation (the Stone's theory) seems to be applicable for all samples. It may be, therefore, concluded that the linear relationship between the spin densities on the oxygens and *g*-values is reliable only in hydrocarbon systems or at the *z*-direction of π-conjugated systems at which s−o interaction is insignificant. If molecules contain heavier atoms such as halogen atoms, moreover, the theory of this study perhaps requires the consideration of the magnitude of s−o coupling constants in the interpretation of the mechanism of substituent effect on *g*-values.

Molecular Structure from the Vewpoint of g-*Tensors.* As has been discussed in this paper, *g*-values contain information from excited states through spin−orbit interactions. On the other hand, molecular structures, as is well-known, also have a close relationship with the excited state, as shown by the Walsh diagram. It can be, therefore, understood that molecular structures should have a strict correlation with the *g*-values. Thus the above-mentioned relation is discussed from the knowledge obtained in this study. In this investigation, it was revealed that the g_x and the g_y of the phenoxyl radical derivatives reflect the contributions of the n−π* and the σ−π* excited states, respectively, through the s−o interactions. It might, furthermore, be considered that, since the larger C−O bond length makes the nonbonding orbital (the p_y orbital of the oxygen) more isolated at the position of the oxygen from the phenyl-ring region and makes the s−o interaction of the n−π* excited-state greater, the larger C−O bond length shows that the g_x increases.[8] On the other hand, it might be also considered that, since the larger C−O bond length reflects that the σ bond of the C−O weakens and makes the s−o interaction of the σ−π* excited-state smaller, the larger C−O bond length shows that the g_y decreases. However, more detailed analysis requires more accurate theoretical calculations and the crystal-structure data of the radicals in the matrixes.

The C−O wagging might be also investigated by the relationship between the *g*-tensors and the excited states. Unfortunately, the calculations conducted in this work are not enough accurate to research this topic. The detailed analysis of the relationship between the *g*-tensors and the C−O wagging through the excited states as a function of the para groups essentially requires more experimental and theoretical studies for the phenoxyl radical derivatives. One of the reasons may be that the C−O wagging is more effectively influenced by the matrix environment than the C−O bond length. Here, those topics, therefore, cannot be discussed any more.

7. Conclusions

This multi-frequency ESR study enabled us to systematically interpret the powder-pattern ESR spectra for a series of phenoxyl radical derivatives that have the *tert*-butyl groups at both ortho positions, achieving the ESR parameters, especially the *g*-tensors. The *g*-tenors of the radicals in this study were proved to essentially show an orthorhombic symmetry. It was found that theoretical quantum-chemical calculations, i.e., the DFT method, successfully reproduce the experimental values. The substituent effect of the para groups on the *g*-tensors, thus, was investigated in detail from the viewpoint of the individual Δg correction term at the tensor level. Futhermore, the spin−orbit interactions were confirmed to be the dominant contributions. With a focus on the s−o term, the mechanism of the influence of the exited states on the *g*-values was furthermore researched by the visualization of the molecular orbitals of the radicals. Finally, the links between the electronic structure or molecular structure and the *g*-values were represented from the knowledge obtained through this study. This study thus shows the significant potential of the combination of a multi-frequency ESR approach and a DFT calculation, especially for investigations of *g*-tensors.

Supporting Information Available: Figure S1−S6, showing the experimental and simulated all-band ESR spectra of the radicals, Table S1, listing the experimental and calculated *g*-tensors, Table S2a, listing the hyperfine-splitting data, Table S2b, listing the isotropic hyperfine-splitting data obtained in the solution experiments, and Table S3, summarizing the detailed breakdowns of the contributions to the *g*-tensors calculated. These materials are available free of charge via the Internet at http://pubs.acs.org.

References and Notes

(1) Stone, A. J. *Proc. R. Soc. London* **1963**, *A271*, 424.
(2) Stone, A. J. *Mol. Phys.* **1963**, *6*, 509.
(3) Kikuchi, O. *Bull. Chem. Soc. Jpn.* **1969**, *42*, 47.
(4) Kikuchi, O. *Bull. Chem. Soc. Jpn.* **1969**, *42*, 1187.
(5) Kawamura, T.; Matsunami, S.; Yonezawa, T.; Fukui, K. *Bull. Chem. Soc. Jpn.* **1965**, *38*, 1935.
(6) Kawamura, T.; Matsunami, S.; Yonezawa, T. *Bull. Chem. Soc. Jpn.* **1967**, *40*, 1111.
(7) Un, S.; Atta, M.; Fontecave, M.; Rutherford, A. W. *J. Am. Chem. Soc.* **1995**, *117*, 10713.
(8) Engstrom, M.; Himo, F.; Agren, H. *Chem. Phys. Lett.* **2000**, *319*, 191.
(9) Frantz, S.; Hartmann, H.; Doslik, N.; Wanner, M.; Kaim, W.; Kummerer, H.-J.; Denninger, G.; Barra, A-L.; Duboc-Toia, C.; Fiedler, J.; Ciofini, I.; Urban, C.; Kaupp, M. *J. Am. Chem. Soc.* **2002**, *124*, 10563.
(10) Frisch, M. J.; Trucks, G. W.; Schlegel, H. B.; Scuseria, G. E.; Robb, M. A.; Cheeseman, J. R.; Montgomery, Jr., J. A.; Vreven, T.; Kudin, K. N.; Burant, J. C.; Millam, J. M.; Iyengar, S. S.; Tomasi, J.; Barone, V.; Mennucci, B.; Cossi, M.; Scalmani, G.; Rega, N.; Petersson, G. A.; Nakatsuji, H.; Hada, M.; Ehara, M.; Toyota, K.; Fukuda, R.; Hasegawa, J.;

Ishida, M.; Nakajima, T.; Honda, Y.; Kitao, O.; Nakai, H.; Klene, M.; Li, X.; Knox, J. E.; Hratchian, H. P.; Cross, J. B.; Bakken, V.; Adamo, C.; Jaramillo, J.; Gomperts, R.; Stratmann, R. E.; Yazyev, O.; Austin, A. J.; Cammi, R.; Pomelli, C.; Ochterski, J. W.; Ayala, P. Y.; Morokuma, K.; Voth, G. A.; Salvador, P.; Dannenberg, J. J.; Zakrzewski, V. G.; Dapprich, S.; Daniels, A. D.; Strain, M. C.; Farkas, O.; Malick, D. K.; Rabuck, A. D.; Raghavachari, K.; Foresman, J. B.; Ortiz, J. V.; Cui, Q.; Baboul, A. G.; Clifford, S.; Cioslowski, J.; Stefanov, B. B.; Liu, G.; Liashenko, A.; Piskorz, P.; Komaromi, I.; Martin, R. L.; Fox, D. J.; Keith, T.; Al-Laham, M. A.; Peng, C. Y.; Nanayakkara, A.; Challacombe, M.; Gill, P. M. W.; Johnson, B.; Chen, W.; Wong, M. W.; Gonzalez, C.; Pople, J. A. *Gaussian 03*, Revision C.02; Gaussian, Inc.: Wallingford, CT, 2004.

(11) Yamaji, T.; Noda, Y.; Yamauchi, S.; Yamauchi, *J. Phys. Chem A* **2006**, *110*, 1196.

(12) Pacifici, J. G.; Browning, H. L., Jr. *J. Am. Chem. Soc.* **1970**, *92*, 5231−5233.

(13) Adachi, A.; Yamauchi, J. *Synth. Met.* **1995**, *73*, 101−105.

(14) Yamauchi, J.; Katayama, A.; Tamada, M.; Tanaka, S. *Appl. Magn. Reson*. **1994**, *6*, 373.

(15) Yamauchi, J.; Yamaji, Y.; Katayama, A. *Appl. Magn. Reson*. **2003**, *25*, 209.

(16) Clough, S.; Poldy, F. *J. Chem. Phys.* **1969**, *51*, 2076.

(17) Malkina, O. L.; Vaara, J.; Schimmelpfenning, B.; Munzarova, M.; Malkin, V. G.; Kaupp, M. *J. Am. Chem. Soc.* **2000**, *122*, 9206.

(18) Bresgunov, A. Y.; Dubinsky, A. A.; Poluektov, O. G.; Lebedev, Y. S.; Prokof'ev, A. I. *Mol. Phys.* **1992**, *75* (5), 1123.

(19) Neese, F. *J. Chem. Phys.* **2001**, *115* (24), 11080.

(20) Kaupp, M.; Buhl, M.; Malkin, V. G. *Calculation of NMR and EPR Parameters: Theory and Applications*; Wiley-VCH: Weinheim, Germany, 2004.

(21) Angstl, R. *Chem. Phys.* **1989**, *132*, 435.

(22) Torring, J. T.; Un, S.; Knupling, M.; Plato, M.; Mobius, K. *J. Chem. Phys.* **1997**, *107* (10), 3905.

(23) Prahananda, B. S. *J. Chem. Phys.* **1983**, *79* (12), 5752.

(24) Zandstra., P. J. *J. Chem. Phys.* **1964**, *41*, 3655.

(25) Koseki, S.; Schmit, M. W.; Gordon, M. S. *J. Phys. Chem.* **1992**, *96*, 10768.

(26) Batra, R.; Giese, B.; Spichty, M.; Gescheidt, G.; Houk, K. N. *J. Phys. Chem.* **1996**, *100*, 18371.

(27) Ohya, H.; Yamauchi, J. *Electron Spin Resonance* (written in Japanese); Koudansha Scientific: Tokyo, 1989; p 114.